Paleoceanography and Paleoclimatology

RESEARCH ARTICLE
10.1029/2019PA003698

Special Section:
Special Collection to Honor the Career of Robert C. Thunell

Reconstructing 800 Years of Carbonate Ion Concentration in the Cariaco Basin Using the Area Density of Planktonic Foraminifera Shells

A. N. Davis[1], C. V. Davis[1], R. C. Thunell[1,2], E. B. Osborne[3], D. E. Black[4], and C. R. Benitez-Nelson[1]

[1]School of the Earth, Ocean, and Environment, University of South Carolina, Columbia, SC, USA, [2]Deceased 30 July 2018, [3]Ocean Acidification Program, National Oceanic and Atmospheric Administration, Silver Spring, MD, USA, [4]School of Marine and Atmospheric Sciences, Stony Brook University, Stony Brook, NY, USA

Key Points:
- Foraminiferal area density serves as a proxy for paleo-$[CO_3^{2-}]$ in the Cariaco Basin showing a 54 μmol kg^{-1} decline since the Industrial Revolution
- Long-term rate of $[CO_3^{2-}]$ change in the Post-Industrial (1760–2007) Cariaco Basin has been double that which occurred during the Medieval Climate Anomaly
- Cariaco Basin $[CO_3^{2-}]$ variability prior to the Industrial Revolution (1760 CE) is characterized by short-term oscillations

Supporting Information:
- Supporting Information S1

Correspondence to:
C. V. Davis,
cvdavis@seoe.sc.edu

Citation:
Davis, A. N., Davis, C. V., Thunell, R. C., Osborne, E. B., Black, D. E., & Benitez-Nelson, C. R. (2019). Reconstructing 800 years of carbonate ion concentration in the Cariaco Basin using the area density of planktonic foraminifera shells. *Paleoceanography and Paleoclimatology*, *34*, 2129–2140. https://doi.org/10.1029/2019PA003698

Received 21 JUN 2019
Accepted 6 DEC 2019
Accepted article online 10 DEC 2019
Published online 19 DEC 2019

Abstract Anthropogenically mediated ocean acidification (OA) has negative impacts on many marine organisms, especially calcifiers. However, systematic measurements of OA have only been made over the past four decades. In order to improve future predictions and understand how ongoing OA compares to natural variability on longer timescales, it is critical to extend records beyond observational time series. In the Cariaco Basin, located in the tropical Atlantic, near-surface dissolved inorganic carbon reflects atmospheric carbon dioxide concentrations (CO_2) since the Industrial Revolution, making it an ideal site for examining longer-term variability. We extend the record of Cariaco Basin near-surface $[CO_3^{2-}]$ back to 1240 CE, using the area density (shell weight (μg)/shell area (μm^2)) of the planktonic foraminifer *Globigerinoides ruber* (pink). Multidecadal variability is observed throughout the record. Since the Industrial Revolution (1760–2007 CE), $[CO_3^{2-}]$ has declined by 0.22 μmol kg^{-1} year^{-1}, in agreement with the magnitude and direction of change captured in the shorter instrumental time series. During the Little Ice Age (1500–1760 CE), a period marked by regional drought, substantial variability but no long-term trend is observed, while a decrease in $[CO_3^{2-}]$ of 0.11 μmol kg^{-1} y^{-1} occurs at the end of the Medieval Climate Anomaly (MCA) (1240 – 1500 CE). Both the MCA and Little Ice Age contain substantial natural variability in near surface $[CO_3^{2-}]$ that we attribute to changes in regional upwelling and atmospheric CO_2. However, the decline in $[CO_3^{2-}]$ occurring in the Post-Industrial Period is anomalous against a backdrop of 800 years of natural variability, reflecting OA associated with anthropogenic increases in atmospheric CO_2.

1. Introduction

Since the advent of the Industrial Revolution in ~1760 CE, the concentration of atmospheric carbon dioxide (CO_2) has increased from ~280 ppm to 415 ppm in 2019 CE (NOAA, 2016; https://www.esrl.noaa.gov/gmd/ccgg/trends/monthly.html; accessed 5/18/19). It is estimated that the oceans have taken up approximately 30% of this anthropogenic CO_2 (DeVries, 2014; Gruber et al., 2019; Khatiwala et al., 2013; Sabine et al., 2004), which has led to an estimated 0.1 unit global decrease in average surface ocean pH (Orr et al., 2005), a process known as ocean acidification (OA). As a result, carbonate ion concentration ($[CO_3^{2-}]$) has decreased by 29 μmol kg^{-1} in the surface waters of the tropical ocean since the Industrial Revolution (~1760 CE) (Orr et al., 2005). Under the AR5 Representative Concentration Pathway 8.5 ("business-as-usual") scenario, average surface pH is predicted to decrease by an additional 0.34 units from 2000 levels by the year 2100 (Gattuso et al., 2015). Several studies have demonstrated that calcifying organisms are negatively impacted by decreased pH, particularly their ability to build and maintain calcium carbonate ($CaCO_3$) structures (Guinotte & Fabry, 2008; Kroeker et al., 2010; Orr et al., 2005; Ries et al., 2009). Reduced calcification rates may have drastic effects on marine ecosystems as many calcifying organisms, such as corals, mollusks, and calcifying algae, provide habitats for other species and protect coastlines from erosion and wave activity (Baco, 2007; Fabry et al., 2008; Guinotte & Fabry, 2008; Moberg & Folke, 1999; Roberts et al., 2006). Moreover, calcifying plankton (i.e., coccolithophores, foraminifera, and pteropods) form the basis of many food webs in the marine environment (Fabry et al., 2008; Guinotte & Fabry, 2008) and play an important role in marine carbon cycling (Schiebel, 2002; Barker et al., 2003; Ridgewell & Zeebe, 2005; Davis et al., 2017).

Instrumental time series provide valuable data needed to study ongoing changes in marine inorganic carbonate chemistry. A compilation of time series data shows OA occurring on a global scale, including

increases in the partial pressure of CO_2 (pCO_2) and dissolved inorganic carbon (DIC), and decreases in pH over the past four decades (Bates et al., 2014). However, the oldest of these time series only began in 1983 (Bates et al., 2014) and global surveys of ocean DIC were only initiated in the 1970s (e.g., GEOSECS; Takahashi et al., 1982). An extension of these records is needed to better understand inherent natural variability of the surface carbonate system. Planktonic foraminifera, a calcifying zooplankton, are commonly used in paleoreconstructions as they have a long fossil record, widespread distribution, and reflect seawater parameters in the geochemistry and morphology of their shells. Proxies such as boron isotopes (Hemming & Hanson, 1992; Sanyal et al., 1996, 2001; Hönisch & Hemming, 2004; Foster & Rae, 2016), B/Ca ratios (Allen et al., 2016; Henehan et al., 2015; Russell et al., 2004; Yu et al., 2007), and size-normalized weight of foraminifera (Barker & Elderfield, 2002; Marshall et al., 2013; Moy et al., 2009; Osborne et al., 2016) have been used to reconstruct seawater carbonate chemistry over decadal to million-year time scales.

The Cariaco Basin, located in the tropical Atlantic Ocean on the continental shelf north of Venezuela, was the site of a long-term observational time series (1996–2018) and is characterized by high sedimentation rates and anoxic bottom waters (Astor et al., 2017). As such, Cariaco Basin sediments contain a rich, high-resolution fossil record, with little bioturbation, which make it a promising location for linking ongoing changes in OA to the historical and geologic record (Hughen et al., 1996). Previous work on the $\delta^{13}C$ of foraminifera from sediment traps and high-resolution sediment cores in the Cariaco Basin has shown a decrease of 0.03‰ $year^{-1}$ and 0.02‰ $year^{-1}$ respectively, between 1996 and 2007, reflective of the global decrease in the $\delta^{13}C$ of CO_2 resulting from the combustion of fossil fuels (the Suess Effect) (Black et al., 2011; Keeling, 1979). Furthermore, Cariaco Basin foraminiferal $\delta^{13}C$ has decreased in response to increasing DIC since the Industrial Revolution, corresponding to an increase in atmospheric CO_2 of ~173 ppm (Black et al., 2011; NOAA, 2016). Together, these results indicate that surface water DIC in Cariaco Basin reflects global atmospheric CO_2 and that foraminifera are a valuable tool for extending records of atmospheric CO_2 in surface waters into the preindustrial age using additional proxy approaches (Astor et al., 2013; Black et al., 2011).

A promising and relatively accessible (low-cost and requiring only an abundance of foraminifera) proxy for near surface seawater [CO_3^{2-}] in the Cariaco Basin is area density, or individual shell weight normalized to 2-D surface area (Marshall et al., 2013). Size-normalizing planktic foraminifera weight reduces environmentally influenced changes in size, such as temperature (Schmidt et al., 2004; Lombard et al., 2009), and has been shown to be a proxy for shell thickness or calcification intensity (Marshall et al., 2013). In the Cariaco Basin, *Globigerinoides ruber* (pink) is present between 0 and 65 m depth year-round, recording near-surface parameters in its shell (de Miró, 1976; Tedesco et al., 2007; Tedesco & Thunell, 2003; Wejnert et al., 2013). A Cariaco Basin sediment trap calibration study conducted by Marshall et al. (2013) carefully evaluated *Globigerinoides ruber* (pink) area density and ambient [CO_3^{2-}] at the depth of calcification to produce the calibration relationship applied in this study. Here, we used area density to reconstruct [CO_3^{2-}] in the Cariaco Basin from 1240–2007 CE, in order to establish a long-term record of both inherent natural variability and anthropogenic forcing and to compare trends and variability in near-surface [CO_3^{2-}] in pre- and post-Industrial time periods in the Cariaco Basin.

1.1. Cariaco Basin

The Cariaco Basin experiences strong seasonal variability due to migration of the Intertropical Convergence Zone (ITCZ), which controls easterly Trade Winds (Muller-Karger & Castro, 1994). When the ITCZ is at its most southerly position (January–April), trade winds are positioned over the basin causing the upwelling of low temperature, high salinity, CO_2-rich, and nutrient-rich Subtropical Underwater to the surface (Morrison & Smith, 1990; Peterson et al., 1991). Northward ITCZ movement (September–December) pushes the easterlies north of the coast, reducing wind strength and upwelling (Astor et al., 2003, 2005; Hughen et al., 1996, 1998). The northward shift also drives an increase in precipitation that increases freshwater input to the basin from local rivers (Astor et al., 2017; Lorenzoni, 2005; Lorenzoni et al., 2009; Peterson & Haug, 2006). Shifts in the position of the ITCZ have been shown to similarly drive Cariaco Basin climate on longer (centennial-millennial) timescales (Haug et al., 2001; Peterson & Haug, 2006).

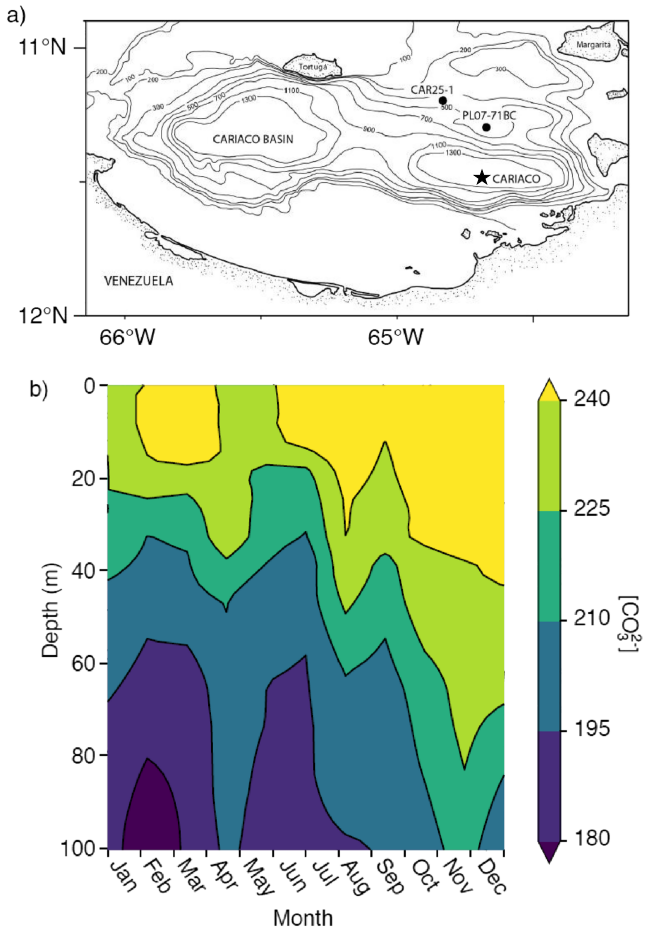

Figure 1. Map (a) of the location of two box cores from the Cariaco Basin (black circles) and (b) smoothed interpolated temperature between the surface and 100 m depth between 1995 and 2018 at the CARIACO station, plotted by day of the year.

From 1995–2018, the Cariaco Basin was the site of the CARIACO oceanographic time series (Muller-Karger et al., 2019). As part of the time series, hydrographic measurements as well as bottle samples were collected to constrain carbonate chemistry. Measurements reveal that between 1996 and 2012, the rate of pCO_2 increase was 2.95 ± 0.43 μatm year^{-1}, DIC increased by 0.64 μmol kg^{-1} year^{-1}, meanwhile pH decreased by 0.0025 year^{-1} and [CO_3^{2-}], calculated from measurements of pH and total alkalinity (TA), decreased by 9.6 μmol kg^{-1} between 1996 and 2017 (Bates et al., 2014; http://www.imars.usf.edu/cariaco; accessed 5/18/19). These trends have been attributed to changes in upwelling of Subtropical Underwater (Bates et al., 2014) as well as global OA. In addition to multidecadal trends, there is evidence of seasonal and interannual variability in [CO_3^{2-}], largely due to upwelling (Astor et al., 2003, 2005; Muller-Karger et al., 2004) (Figure 1 and supporting information Figure S1).

2. Materials and Methods

The two box cores used in this study were collected in 1990 and 2008 from the Cariaco Basin: PL07-71-BC (10°36.06°N, 64°39.60°W) from a depth of 449 m, and CAR25-1 (10°45.98°N, 64°46.20°W) from a depth of 450 m (Figure 1). PL07-71-BC was dated between 1239 and 1990 CE using ^{14}C ages from *Globigerina bulloides* combined with astronomical tuning for sediment pre-1880, and varve counts along with ^{210}Pb prior to 1880 (Black et al., 1999, 2009). The upper portion of CAR25-1 used in this study spans 1984–2008 CE and was dated using ^{210}Pb to within ±4–6 years. Both cores were sampled at 1 mm intervals at approximately annual resolution (Black et al., 2011). The sampled sections were rinsed over a 150 μm mesh sieve for foraminiferal analyses.

Up to 40 *G. ruber* (pink) were picked from the 1 mm interval dated to the turn of each decade. Where fewer than 40 foraminifera were available, additional individuals were picked from 1–2 mm both above and below and pooled such that each sample consists of foraminifera (average n = 31) from 1–5 mm of sediment centered around the turn of the decade. The need to frequently pool multiple core intervals to reach the target number of individual foraminifera results in a decadally resolved data set. Care was taken to select foraminifera that had intact tests and no visible debris attached. Each individual *G. ruber* was weighed on a high precision microbalance (Mettler-Toledo XP2U; ±0.43 μg) and photographed umbilical side up using a binocular microscope (Zeiss Stemi 2000-C) with a mounted camera (Point Grey Research Flea3 1394b), following established methodology (Marshall et al., 2013; Osborne et al., 2016). The area of each *G. ruber* was determined with the software Orbiucle Macnification 2.0, which uses RGB imaging to determine the area of each foraminifer in pixels. Pixels were converted to μm^2 using an image of a 1 mm stage micrometer that was taken under the same microscope settings as the foraminifera photos (Marshall et al., 2013; Osborne et al., 2016). Area density values were calculated for each *G. ruber* by dividing the individual foraminifer mass by area (equation (1)).

$$\text{Area Density}\left(\frac{\mu g}{\mu m^2}\right) = \frac{\text{weight }(\mu g)}{\text{area }(\mu m^2)} \quad (1)$$

Area density values were then used to determine [CO_3^{2-}] using the *G. ruber* (pink) relationship developed by Marshall et al. (2013) (equation (2)).

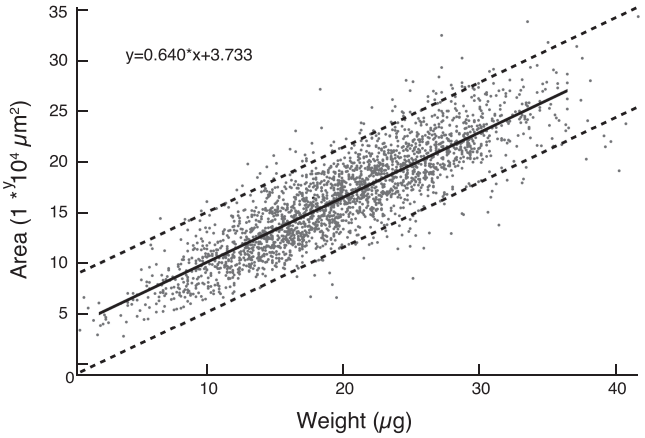

Figure 2. Model II OLS regression with 95% confidence intervals (dashed lines) demonstrating the good correlation ($R^2 = 0.75$; p value < 0.001) between the measured weight and area of the *G. ruber* (pink) foraminifera.

$$Area\ Density\left(\frac{\mu g}{\mu m^2}\right)*10^{-4} = (0.119\pm0.24) + (0.00442\pm0.001)*\left[CO_3^{2-}\right]\left(\frac{\mu mol}{kg}\right) \quad (2)$$

Area density measurements have a propagated error of 2.2%, based on repeated measurements of both weight and area, much smaller than the standard error plotted hereafter. Total Alkalinity (±2 μmol kg^{-1}) and pH (±0.001) measurements along with corresponding temperature, salinity, and depth from the CARIACO time series were used to calculate [CO_3^{2-}] with the CO2SYS program (Lewis et al., 1998) using Mehrbach et al. (1973) constants updated by Dickson and Millero (1987). Concentrations of phosphate and silicate were not used in these calculations. The time series spans 1996–2018 with data gaps due to missing hydrographic data (supporting information Figure S1).

Statistical analyses of correlations between area density derived [CO_3^{2-}] and other proxies were carried out using Spearman's correlation, to account for nonnormality in the distribution of [CO_3^{2-}] within time periods. In each case, the Holm method was used to correct for multiple hypothesis testing (Holm et al., 1979). All statistics were conducted using the base and "psych" packages in R (R Core Team, 2018; Revelle, 2018).

3. Results

3.1. Morphometric Characteristics

Area and weight data generated for 2,418 individual *G. ruber* (pink) show a good linear correlation ($R^2 = 0.75$; p value < 0.001; Figures 2 and 3), indicating that size normalization effectively accounts for most changes in weight due to growth. The highly significant relationship between size and weight also shows that factors such as secondary precipitation, dissolution, or sediment infilling were minimal or consistent through time. However, scatter within this relationship does demonstrate variability in the size and weight relationship for any given individual foraminifera, such as the influence of body size on response to carbonate chemistry (Henehan et al., 2017) or the influence of temperature and nutrients during an individual's lifetime. Moreover, no significant relationship was found between sample average area density and average area (p value = 0.24), indicating that size normalization of weights was effective in limiting bias due to size change.

Richey et al. (2019) recently showed that there are two morphotypes of *G. ruber* (pink), corresponding to the sensu stricto and sensu latu morphotypes of *G. ruber* (white). While previous studies have shown that calcification can vary significantly between morphotypes (Marshall et al., 2015; Osborne et al., 2016), the Marshall et al. (2013) relationship, generated prior to the recognition of *G. ruber* (pink) morphotypes, proved robust without distinguishing between the two. Therefore, although both *G. ruber* (pink) morphotypes were observed in this record, we have followed the methodology of Marshall et al. (2013) in not considering the two morphologies separately.

3.2. [CO_3^{2-}] Record

Our decadally resolved [CO_3^{2-}] record spans 1240–2007 CE (Figure 4) and can be divided into three periods based on local trends that largely coincide with widespread climatic shifts: the Medieval Climate Anomaly (MCA; 1240–1500 CE), the Little Ice Age (LIA; 1500–1760 CE), and the Post-Industrial Period (PIP; 1760-2007 CE).

3.2.1. Post-Industrial Period

Sample average nonnormalized weights and shell size (2-D area) are variable throughout the PIP (Figure 3). While nonnormalized weights and shell size covary closely within a sample, there is an overall increase in shell size over the course of the PIP that is not clearly reflected in shell weight (Figure 2). Size normalization of shell weights results in a relatively constant area density between 1760 and 1820, followed by a steady decrease continuing to the end of the record in 2007 (Figure 3). Converting area density into [CO_3^{2-}]

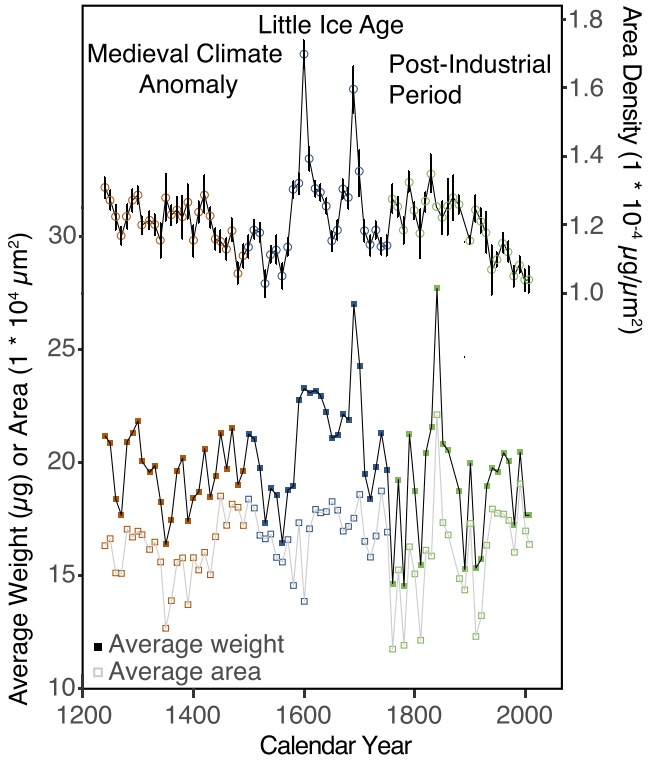

Figure 3. Decadally resolved average area density (μg/μm^2), nonnormalized weight (μg) and cross-sectional surface area (μm^2) of *G. ruber* (pink). Vertical error bars represent standard error for each sample; horizontal error bars are smaller than the points. Colors denote the Medieval Climate Anomaly (1240–1500 CE; red line), Little Ice Age (1500–1760 CE; blue line), and Post-Industrial Period (1760–2007, green line).

shows values ranging from 279 μmol/kg in the year 1820 to 202 μmol/kg in 1990. Over the span of the PIP, this results in an overall decrease of 54 μmol/kg from 268 to 214 μmol/kg representing a 20% decline and an average rate of decrease of 0.22 μmol kg^{-1} year^{-1} (Figure 4).

3.2.2. LIA

Through the LIA, *G. ruber* (pink) shell size remains relatively constant, while average nonnormalized weight increases between 1590 and 1700 (Figure 3). Although this trend is apparent in nonnormalized weights and sizes, it does not represent a significant departure from the relationship between weight and size observed from other time periods (Figure 4). In terms of area-density derived [CO_3^{2-}], the LIA is marked by high variability with values ranging from 206 to 357 μmol kg^{-1}. Two maxima are prominent at 1600 and 1690 CE. Both peaks have a similar shape, flanked by other high [CO_3^{2-}] values, and occur over several decades. Despite substantial decadal-scale variability, there was no significant trend in [CO_3^{2-}] during the LIA (p value = 0.45) (Figure 4).

3.2.3. Medieval Climate Anomaly

Both nonnormalized weight and size covary closely through the MCA, increasing slightly after ~1420 CE (Figure 3). The [CO_3^{2-}] values calculated for the MCA are the least variable of the three time periods, ranging between just 232 and 260 μmol/kg. There is an overall decrease in [CO_3^{2-}] during the MCA that averaged 0.11 μmol kg^{-1} year^{-1}. The overall decrease largely occurs during the latter part of the record from 1420–1500 CE where there is a steeper decrease in [CO_3^{2-}] of 0.42 μmol kg^{-1} year^{-1} (Figure 4).

3.3. [CO_3^{2-}] Comparison to Mg/Ca Temperature, *G. bulloides* Abundance, and CO_2 Records

The reconstructed [CO_3^{2-}] record is compared to temperatures calculated from *G. ruber* Mg/Ca ratios (Figure 5c; Wurtzel et al., 2013), and *G. bulloides* abundance, a proxy for upwelling (Figure 5d; Black et al., 1999), measured from the same cores. In addition, records are compared to atmospheric CO_2 measured from the Law Dome ice core (Figure 5e; Etheridge et al., 1998; https://cdiac.ess-dive.lbl.gov/ftp/trends/co2/lawdome.combined.dat), chosen as this record has been shown previously to correlate well with $\delta^{13}C$ measured in shallow-water Caribbean sclerosponges (Böhm et al., 2002).

Directly comparing the entire length of the [CO_3^{2-}] record to Mg/Ca, *G. bulloides* abundance, and atmospheric CO_2, shows that [CO_3^{2-}] has a small but significant negative correlation with Mg/Ca temperatures (Spearman rho = −0.04; p value < 0.01), *G. bulloides* abundance (Spearman rho = −0.29; p value = 0.01), and atmospheric CO_2 (Spearman rho = −0.33; p value < 0.01). In the PIP, [CO_3^{2-}] values are significantly correlated only with atmospheric CO_2 (Spearman rho = −0.62; p value < 0.01; Figure S2c). During the LIA, [CO_3^{2-}] correlates with both atmospheric CO_2 (Spearman rho = −0.66; p value < 0.01; Figure S2c) and the abundance of *G. bulloides* (Spearman rho = −0.45; p value = 0.02; Figure S2b). Medieval Climate Anomaly [CO_3^{2-}] values only show a significant correlation with the abundance of *G. bulloides* (Spearman rho = −0.41; p value = 0.03; Figure S2b).

4. Discussion

Our eight-century Cariaco Basin [CO_3^{2-}] record is broken into three time periods based on relevant natural and anthropogenic climate perturbations observed here and previously described by Black et al. (2004, 2007): the MCA (1240–1500), the LIA (1500–1760), and the PIP (1760–2007). In the Northern Hemisphere, the MCA is characterized by widespread warmer temperatures (Mann et al., 2009), while the LIA is marked by larger glaciers, more sea ice, lower snowlines, and lower temperatures (Bond et al., 1997; Grove, 1988; Keigwin, 1996; Mann et al., 2009). The PIP is defined by the start of the Industrial

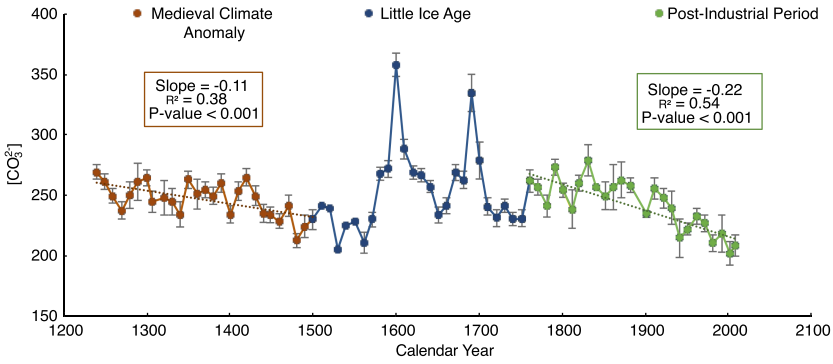

Figure 4. Decadally resolved carbonate ion concentration ($[CO_3^{2-}]$) from 1240–2007 CE divided into three periods: Medieval Climate Anomaly (1240–1500 CE; red line), Little Ice Age (1500–1760 CE; blue line), and Post-Industrial Period (1760–2007, green line). From 1240–1560 CE, there is a decrease of 0.11 μmol kg^{-1} $year^{-1}$ ($R^2 = 0.51$; p value < 0.001). During the Little Ice Age, there was no statistically significant trend in $[CO_3^{2-}]$ (p value $= 0.45$). From 1760–2007 CE, there is a decrease of 0.22 μmol kg^{-1} $year^{-1}$ ($R^2 = 0.54$; p value < 0.001). Vertical error bars represent standard error for each sample; horizontal error bars are smaller than the points.

Revolution. Based on modern observations of seasonal to interannual variability, near-surface $[CO_3^{2-}]$ in the Cariaco Basin would be expected to respond to three primary factors: (1) variations in atmospheric CO_2; (2) the upwelling of deep, CO_2-rich waters into the surface; and (3) sea surface temperature, which can cause an increase in CO_2 outgassing of 16 to 20 μatm per 1 °C increase in the Cariaco Basin (Astor et al., 2013; Gordon & Jones, 1973; Takahashi et al., 1993).

Several variables, in addition to $[CO_3^{2-}]$, have been shown to impact size-normalized weight in foraminifera more broadly, including preservation and dissolution (Broecker & Clark, 2001; Lohmann, 1995), temperature, productivity, and optimum growth conditions (e.g., Aldridge et al., 2012; De Villiers, 2004; Marshall et al., 2013; Naik et al., 2011; Naik et al., 2013; Weinkauf et al., 2016). At the depth of our core sites, water is supersaturated with respect to carbonate ($\mathbf{\Omega}$ =1.7 at 500 m) making significant dissolution unlikely. On seasonal time scales, where upwelling is a major driver of seasonality, $[CO_3^{2-}]$, temperature, and $[PO_4^{3-}]$ are correlated, with area density showing a positive relationship with the former two variables, and a negative relationship with the later. In the development of the area-density proxy applied here, Marshall et al. (2013) analyzed the relationships between area density, $[CO_3^{2-}]$, temperature, and $[PO_4^{3-}]$, and determined that 89% of the variability in modern-day area density values of *G. ruber* (pink) is attributable to $[CO_3^{2-}]$ and that neither temperature nor $[PO_4^{3-}]$ are confounding variables. While these variables correlate seasonally, this is not necessarily the case on longer time scales (Figures 5 and S2). Osborne et al. (2016) showed that where temperature and $[CO_3^{2-}]$ trends diverge on longer time scales in Santa Barbara Basin, $[CO_3^{2-}]$ is the more important driver of area density. Similarly, over the course of the CARIACO time series, $[CO_3^{2-}]$ and primary productivity have decreased, while temperature has increased (Muller-Karger et al., 2019; Taylor et al., 2019); thus, these latter two variables cannot be the primary drivers of area density over this interval. These lines of evidence all support the use of area density as a proxy to reconstruct long-term trends in $[CO_3^{2-}]$ in this setting.

4.1. Post-Industrial Period

The subsurface $[CO_3^{2-}]$ record from foraminiferal area density is largely in agreement with instrumental data from surface waters (<5 m depth) in both the Cariaco Basin (CARIACO) and the tropical Pacific (HOTS); (Dore et al., 2009; http://hahana.soest.hawaii.edu/hot/products/HOT_surface_CO2.txt), despite a substantial difference in resolution (decadal versus < monthly) (Figure 6). Records from the CARIACO and HOT time series showed rates of $[CO_3^{2-}]$ decrease of 0.46 and 0.49 μmol kg^{-1} $year^{-1}$ in surface waters, between 1996–2017 and 1988–2016, respectively, reflecting global trends in atmospheric CO_2 (Figure 6). By comparison, our area density record shows a decrease in $[CO_3^{2-}]$ of 0.58 μmol kg^{-1} $year^{-1}$ between 1990 and 2007. Although the trend in the area density record is consistent in direction and comparable in magnitude, absolute $[CO_3^{2-}]$ values are lower than those from the surface water CARIACO or HOT time series

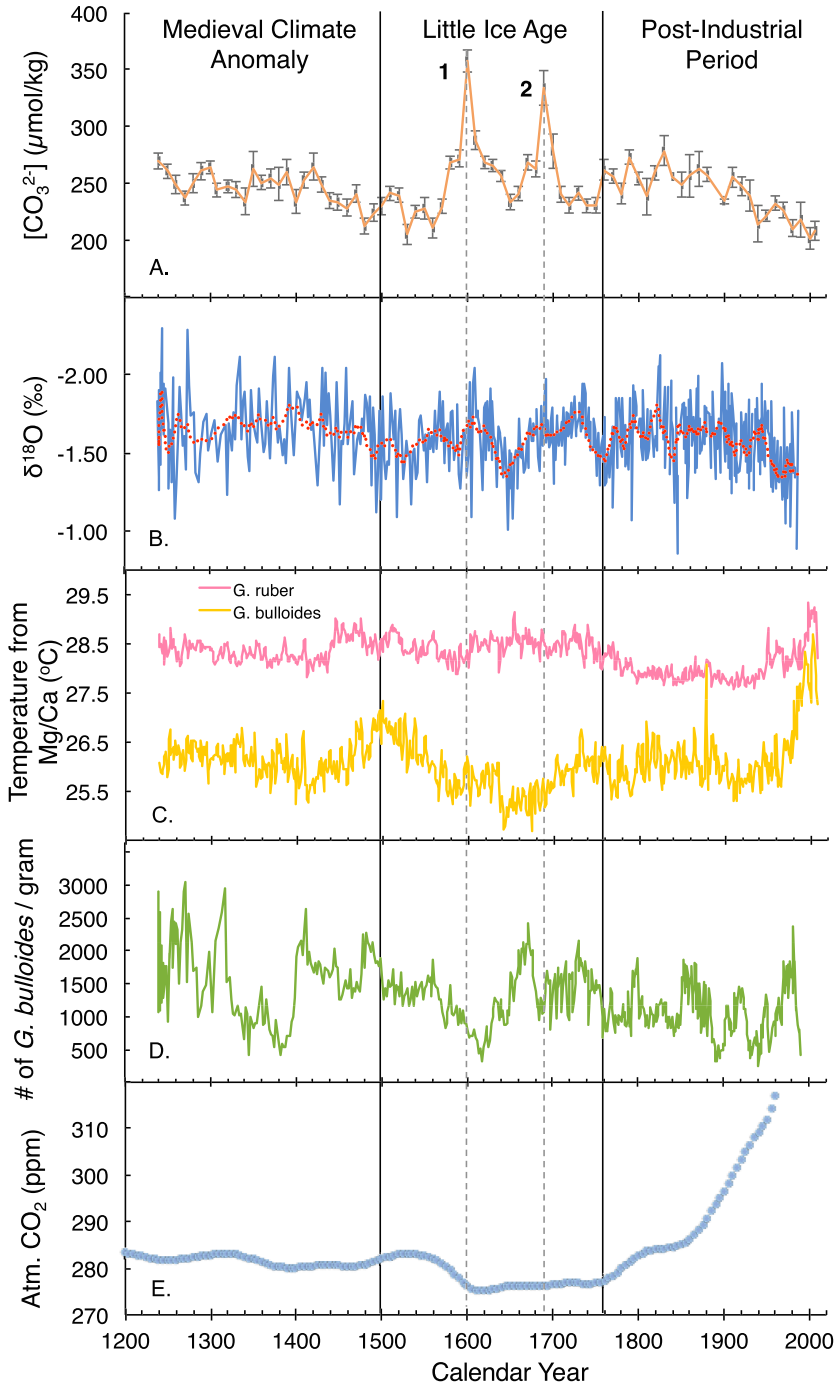

Figure 5. Comparison of Cariaco Basin (a) $[CO_3^{2-}]$ (orange line), with error bars representing standard error, (b) *G. ruber* (pink) $\delta^{18}O$ (blue line with 10 period moving average in red; Black et al., 2004), (c) temperature calculated from *G. ruber* (pink) Mg/Ca (biased toward nonupwelling conditions) and *G. bulloides* (yellow) Mg/Ca (biased toward upwelling conditions) (Black et al., 2007; Wurtzel et al., 2013), (d) *G. bulloides* abundance, a proxy for upwelling (green line; Black et al., 1999), and (e) atmospheric CO_2 concentrations measured from the Law Dome Ice Core (light blue circles; Etheridge et al., 1998). Numbers 1 and 2 denote decades of high $[CO_3^{2-}]$ during 1600 and 1690 CE, with dark lines delineating the three time periods, the MCA, LIA, and PIP.

(Figure 6), a reflection of the subsurface calcification environment of *G. ruber* (pink). Some previous studies show *G. ruber* calcifying as deep as 65 m (Bé, 1982; Rebotim et al., 2017; Tedesco et al., 2007), and *G. ruber* values fall within the measured $[CO_3^{2-}]$ range of their proposed depth habitat of 1-65 m within the Cariaco

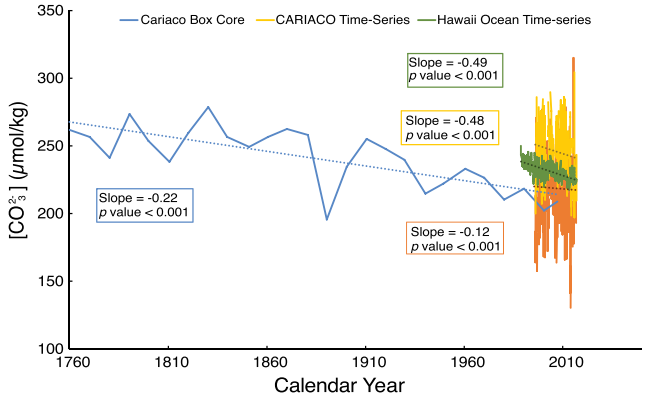

Figure 6. Comparison of postindustrial [CO_3^{2-}] records from Cariaco Basin including the box core reconstruction (dark blue line) and surface CARIACO time series data (>5 m depth; yellow line), 55 m depth CARIACO time series (light blue line), and surface Hawaii Ocean Time series (HOT; <5 m depth; green line). Note that slopes refer to different lengths of record.

Basin (Figure 6), and close to [CO_3^{2-}] values from 25 m depth, or an average of 27 μmol kg^{-1} below 1 m values (Figure S1).

The PIP is defined by the onset of industrial carbon emissions to the atmosphere, which has led to a global increase in atmospheric CO_2 of 137 ppm between 1760 and 2019 (Etheridge et al., 1998; NOAA, 2016). The decreasing trend in $\delta^{13}C$ of *G. ruber* (pink) during this interval (Black et al., 2011) demonstrates that anthropogenic forcing has also significantly altered the carbonate chemistry of Cariaco Basin in proportion to the global rise in CO_2. Black et al. (2011) estimated that the ~100 ppm increase in atmospheric CO_2 between 1760 and 1999 would produce a 60 μmol kg^{-1} decrease in surface [CO_3^{2-}]. Our results are in remarkable agreement with this prediction, showing a 54 μmol kg^{-1} decrease in [CO_3^{2-}] during the PIP at an average rate of decrease of 0.22 μmol kg^{-1} $year^{-1}$. Taken together, the agreement between multiple long-term records and recent observational records support a robust signal of ongoing OA in Cariaco Basin, and further validates the utility of the area density [CO_3^{2-}] proxy in generating even longer climate records.

While the increase in atmospheric CO_2 has been dramatic since the Industrial Revolution (Etheridge et al., 1998; NOAA, 2016), upwelling as indicated by *G. bulloides* abundance has remained relatively stable, with some interdecadal variability (Figure 5). Temperature from foraminiferal Mg/Ca ratios was relatively stable through the 1800s, with a prominent increase starting in 1910 and extending to the end of the record (Black et al., 2007; Wurtzel et al., 2013). Comparing our [CO_3^{2-}] record to each of these variables, however, shows a significant correlation only with rising atmospheric CO_2 (Figure S2). Combined, this suggests that the local influences of temperature or upwelling on [CO_3^{2-}] are not as important to long-term change in postindustrial [CO_3^{2-}] as the increase in atmospheric CO_2.

4.2. LIA

Caribbean SSTs during the LIA are cooler than in the MCA and are punctuated by two cold pulses, which are reflected in the Mg/Ca measured in the deeper living *G. bulloides* (biased toward upwelling conditions), but not in surface Mg/Ca temperatures derived from *G. ruber* (Haase-Schramm et al., 2003; Black et al., 2004; Figure 5). Atmospheric CO_2 declines around 1560 to a relatively stable range of 275 to 281 ppm (Figure 5). This period is also associated with a southward migration of the ITCZ, which led to widespread aridity and drought conditions in the Cariaco Basin (Haug et al., 2001; Peterson & Haug, 2006) and surrounding areas (Haug et al., 2003; Hodell et al., 2005; Lane et al., 2011). Haug et al. (2001) demonstrated peak drought conditions in the Cariaco Basin at 1567 CE, 1650 CE, and 1738 CE. Upwelling intensity decreased from 1500–1618 CE then increased until 1672 CE (Black et al., 2007; Figure 5). Water temperatures do not correlate with [CO_3^{2-}]. Rather a decrease in atmospheric CO_2 occurring at ~1600 CE is coincident with an overall increase in [CO_3^{2-}], after which decadal-scale increases in upwelling negatively correlate with our [CO_3^{2-}] record.

The most prominent features in our [CO_3^{2-}] record during the LIA are two large peaks at 1600 and 1690 CE Both coincide with periods of reduced upwelling and productivity, evidenced by decreased abundance of *G. bulloides* (Figure 5; Black et al., 2007), but occur between periods of maximal drought as reported by Haug et al. (2001). A decrease in upwelling simultaneously occurring with a weakening of drought conditions in the Cariaco Basin suggests a northward movement of the ITCZ, as seen on decadal timescales in the modern Cariaco Basin (Taylor et al., 2019). This hypothesis is further supported by regional records showing a temporary increase in precipitation at the beginning and end of the seventeenth century (Hodell et al., 2005). We therefore propose that the two pulses of apparent high [CO_3^{2-}] determined from area density derive from a reduction in physical upwelling processes that seasonally expose *G. ruber* to colder, deeper CO_2 rich waters and higher productivity during multidecadal northward migrations of the ITCZ.

4.3. Medieval Climate Anomaly

The end of the MCA was the most recent period during which a long-term trend in $[CO_3^{2-}]$ has been identified, with a decrease of 0.11 μmol kg^{-1} $year^{-1}$ between 1240 and 1500. Both atmospheric CO_2 and Cariaco Basin near-surface $[CO_3^{2-}]$ were less variable through the late MCA relative to the LIA and PIP (Figure 5). An increase in temperature is evident in Mg/Ca records from 1410–1500 CE (Black et al., 2004, 2007; Wurtzel et al., 2013). Warming at the very end of the MCA corresponds with a decrease in $[CO_3^{2-}]$ (Figures 4 and 5). However, when taking the interval prior to the LIA as a whole, only upwelling is significantly correlated, and thus a likely long-term driver of near-surface $[CO_3^{2-}]$ (Figure 5). Ice core based atmospheric CO_2 concentrations remain relatively constant throughout this period, between 280 and 283 ppm (Etheridge et al., 1998). Upwelling is variable, with periods of increased upwelling from 1240–1360 CE and 1410–1500 CE and decreased upwelling around 1380 CE $[CO_3^{2-}]$ had the strongest correlation with upwelling intensity during this MCA, resulting in reduced $[CO_3^{2-}]$ during periods of more intense upwelling and vice versa (Figure S2).

4.4. Drivers of $[CO_3^{2-}]$ Variability Pre- and Post-Industrialization

Near-surface $[CO_3^{2-}]$ over the past 800 years has been impacted by atmospheric CO_2, local upwelling, and to a lesser extent, changing surface temperature. However, it is important to note that the magnitude of these competing and interrelated influences have varied considerably through the various climatic periods. Prior to the Industrial Revolution the $[CO_3^{2-}]$ of near-surface waters in the Cariaco Basin appears to be sensitive to both shifts in atmospheric CO_2 (LIA) and variations in local upwelling (MCA and LIA), with elevated $[CO_3^{2-}]$ coinciding with periods of reduced upwelling. Between 1240 and 1760, shifts in atmospheric CO_2 were minimal (Figure 5), and high-amplitude variability in $[CO_3^{2-}]$ on decadal timescales is likely linked to changes in upwelling and aridity driven by migration of the ITCZ. In contrast, PIP $[CO_3^{2-}]$ in the Cariaco Basin strongly correlates with the rapid increase in atmospheric CO_2, suggesting that this is the major driver of the ongoing $[CO_3^{2-}]$ decrease in the Cariaco Basin. Elevated CO_2 levels and to a lesser extent, increasing temperature have resulted in the PIP experiencing a doubling in the rate of $[CO_3^{2-}]$ decrease relative to the MCA (p value < 0.05).

Natural variability occurs in preindustrial records of $[CO_3^{2-}]$, but the addition of anthropogenic forcing from elevated atmospheric CO_2 concentrations has been a key driver in the decline in $[CO_3^{2-}]$ since 1760. This trend is comparable in both direction and magnitude with other records of OA in the tropics (Black et al., 2011; HOTS; CARIACO). Our record shows the lowest near-surface $[CO_3^{2-}]$ values observed since the end of the MCA occurring between 1980 and 2007, the most recent decades included in our 800-year record. Moreover, the observed decrease in $[CO_3^{2-}]$ is expected to continue and even accelerate as atmospheric CO_2 continues to increase, potentially leaving calcifiers and ecosystems vulnerable to extremes generated by natural variability, as observed in the preindustrial period, superimposed on a new baseline of low $[CO_3^{2-}]$. These data sets confirm that while short-term local fluctuations in near-surface $[CO_3^{2-}]$ have been the norm in Cariaco Basin, the long-term and rapid decrease observed since the Industrial Revolution is outside the scope of these natural fluctuations, rather reflecting the global increase in CO_2.

5. Conclusions

A decadally resolved reconstruction of surface $[CO_3^{2-}]$ from the area density of *G. ruber* (pink) in the Cariaco Basin provides a long-term record (1240–2007 CE) useful for understanding the impact of inherent natural variability and anthropogenic forcing on the inorganic carbonate system. This record is divided into three periods based on local trends that largely coincide with widespread climatic shifts: the MCA (1240–1500 CE), the LIA (1500–1760 CE), and the PIP (1760–2007 CE). In the Cariaco Basin $[CO_3^{2-}]$ decreased at a rate of 0.11 μmol kg^{-1} $year^{-1}$ during the MCA (1240–1500 CE), with most variation linked to shorter-term fluctuations in upwelling. During the LIA (1500–1760 CE), there is no long-term trend in $[CO_3^{2-}]$, but there are large multidecadal oscillations in $[CO_3^{2-}]$, corresponding to changes in atmospheric CO_2 as well as local upwelling and regional climate change tied to the migration of the ITCZ. The PIP (1760–2007 CE) has experienced a decrease of 54 μmol kg^{-1} at a rate of 0.22 μmol kg^{-1} $year^{-1}$, attributed to increasing carbon emissions over the past two and a half centuries, double the rate of change during the MCA or LIA. The trend in declining $[CO_3^{2-}]$ over the PIP is in close agreement with local in situ time series and with the decrease in near-surface $[CO_3^{2-}]$ since the Industrial Revolution

predicted by Black et al. (2011). As atmospheric CO_2 continues to increase, our record suggests that the rate of $[CO_3^{2-}]$ decrease will continue to accelerate as evidenced by comparisons between reconstruction and instrumental time series data in the Cariaco Basin. Thus, while multidecadal variability in Cariaco Basin $[CO_3^{2-}]$ has been present for at least the past 800 years, the ongoing long-term trend in $[CO_3^{2-}]$ is distinct from these short-term fluctuations.

Acknowledgments
Area density and the resulting $[CO_3^{2-}]$ records are available in the Pangaea data repository online (https://doi.pangaea.de/10.1594/PANGAEA.908054). This work was supported by the National Science Foundation OCE-1631977 (C. B. N., R. T., C. D., and A. C.) and a University of South Carolina Honors College Science Undergraduate Research Fellowship (A. D.). We would like to thank M. Weinkauf and an anonymous reviewer for their thoughtful reviews of this manuscript.

References

Aldridge, D., Beer, C. J., & Purdie, D. A. (2012). Calcification in the planktonic foraminifera Globigerina bulloides linked to phosphate concentrations in surface waters of the North Atlantic Ocean. *Biogeosciences*, *9*(5), 1725–1739. https://doi.org/10.5194/bg-9-1725-2012

Allen, K. A., Hönisch, B., Eggins, S. M., Haynes, L. L., Rosenthal, Y., & Yu, J. (2016). Trace element proxies for surface ocean conditions: A synthesis of culture calibrations with planktic foraminifera. *Geochimica et Cosmochimica Acta*, *193*, 197–221. https://doi.org/10.1016/j.gca.2016.08.015

Astor, Y., Muller-Karger, F., & Scranton, M. I. (2003). Seasonal and interannual variation in the hydrography of the Cariaco Basin: Implications for basin ventilation. *Continental Shelf Research*, *23*(1), 125–144. https://doi.org/10.1016/S0278-4343(02)00130-9

Astor, Y. M., Lorenzoni, L., Guzman, L., Fuentes, G., Muller-Karger, F., Varela, R., et al. (2017). Distribution and variability of the dissolved inorganic carbon system in the Cariaco Basin, Venezuela. *Marine Chemistry*, *195*, 15–26. https://doi.org/10.1016/j.marchem.2017.08.004

Astor, Y. M., Lorenzoni, L., Thunell, R., Varela, R., Muller-Karger, F., Troccoli, L., et al. (2013). Interannual variability in sea surface temperature and fCO_2 changes in the Cariaco Basin. *Deep Sea Research Part II: Topical Studies in Oceanography*, *93*, 33–43. https://doi.org/10.1016/j.dsr2.2013.01.002

Astor, Y. M., Scranton, M. I., Muller-Karger, F., Bohrer, R., & García, J. (2005). fCO_2 variability at the CARIACO tropical coastal upwelling time series station. *Marine Chemistry*, *97*, 245–261. https://doi.org/10.1016/j.marchem.2005.04.001

Baco, A. R. (2007). Exploration for deep-sea corals on North Pacific seamounts and islands. *Oceanography*, *20*(4), 108–117, Retrieved from. http://www.jstor.org.pallas2.tcl.sc.edu/stable/24860153

Barker, S., & Elderfield, H. (2002). Foraminiferal calcification response to glacial-interglacial changes in atmospheric CO_2. *Science*, *297*(5582), 833–836. https://doi.org/10.1126/science.1072815

Barker, S., Higgins, J. A., & Elderfield, H. (2003). The future of the carbon cycle: review, calcification response, ballast and feedback on atmospheric CO_2. *Philosophical Transactions of the Royal Society A*, *361*(1081). https://doi.org/10.1098/rsta.2003.1238

Bates, N., Astor, Y., Church, M., Currie, K., Dore, J., Gonaález-Dávila, M., et al. (2014). A time-series view of changing ocean chemistry due to ocean uptake of anthropogenic CO_2 and ocean acidification. *Oceanography*, *27*(1), 126–141. https://doi.org/10.5670/oceanog.2014.16

Bé, A. W. (1982). Biology of planktonic foraminifera. *Studies in Geology, Notes for a Short Course*, *6*, 51–89. https://doi.org/10.1017/S0271164800000506

Black, D., Thunell, R., Wenert, K., & Astor, Y. (2011). Carbon isotope composition of Caribbean Sea surface waters: Response to the uptake of anthropogenic CO_2. *Geophysical Research Letters*, *38*, L16609. https://doi.org/10.1029/2011GL048538

Black, D. E., Abahazi, M. A., Thunell, R. C., Kaplan, A., Tappa, E. J., & Peterson, L. C. (2007). An 8-century tropical Atlantic SST record from the Cariaco Basin: Baseline variability, twentieth-century warming, and Atlantic hurricane frequency. *Paleoceanography*, *22*, PA4204. https://doi.org/10.1029/2007PA001427

Black, D. E., Hameed, S., & Peterson, L. C. (2009). Long-term tidal cycle influences on a late Holocene clay mineralogy record from the Cariaco Basin. *Earth and Planetary Science Letters*, *279*, 139–146. https://doi.org/10.1016/j.epsl.2008.12.040

Black, D. E., Peterson, L. C., Overpeck, J. T., Kaplan, A., Evan, M. N., & Kashgarian, M. (1999). Eight centuries of North Atlantic Ocean atmosphere variability. *Science*, *286*(5445), 1709–1713. https://doi.org/10.1126/science.286.5445.1709

Black, D. E., Thunell, R. C., Kaplan, A., Peterson, L. C., & Tappa, E. J. (2004). A 2000-year record of Caribbean and tropical North Atlantic hydrographic variability. *Paleoceanography*, *19*, PA2022. https://doi.org/10.1029/2003PA000982

Böhm, F., Haase-Schramm, A., Eisenhauer, A., Dullo, W. C., Joachimski, M. M., Lehnert, H., & Reitner, J. (2002). Evidence for preindustrial variations in the marine surface water carbonate system from coralline sponges. *Geochemistry, Geophysics, Geosystems*, *3*(3), 1019. https://doi.org/10.1029/2001GC000264

Bond, G., Showers, W., Cheseby, M., Lotti, R., Almasi, P., deMenocal, P., et al. (1997). A pervasive millennial-scale cycle in North Atlantic Holocene and glacial climates. *Science*, *278*(5341), 1257–1266. https://doi.org/10.1126/science.278.5341.1257

Broecker, W., & Clark, E. (2001). A dramatic Atlantic dissolution event at the onset of the last glaciation. *Geochemistry, Geophysics, Geosystems*, *2*(11). https://doi.org/10.1029/2001GC000185

Davis, C. V., Rivest, E. B., Hill, T. M., Gaylord, B., Russell, A. D., & Sanford, E. (2017). Ocean acidification compromises a planktic calcifier with implications for global carbon cycling. *Scientific Reports*, *7*, 2225.

de Miró, M. D. (1976). Los foraminíferos planctónicos vivos y sedimentados del margen continental de Venezuela. *Investigación Pesquera (Barcelona)*, *40*(1), 261–319.

De Villiers, S. (2004). Optimum growth conditions as opposed to calcite saturation as a control on the calcification rate and shell-weight of marine foraminifera. *Marine Biology*, *144*(1), 45–49. https://doi.org/10.1007/s00227-003-1183-8

DeVries, T. (2014). The oceanic anthropogenic CO_2 sink: Storage, air-sea fluxes, and transports over the industrial era. *Global Biogeochemical Cycles*, *28*, 631–647. https://doi.org/10.1002/2013GB004739

Dickson, A., & Millero, F. (1987). A comparison of the equilibrium constants for the dissociation of carbonic acid in seawater media. *Deep Sea Research Part A. Oceanographic Research Papers*, *34*(10), 1733–1743. https://doi.org/10.1016/0198-0149(87)90021-5

Dore, J. E., Lukas, R., Sadler, D. W., Church, M. J., & Karl, D. M. (2009). Physical and biogeochemical modulation of ocean acidification in the central North Pacific. *Proceedings of the National Academy of Sciences*, *106*, 12,235–12,240. https://doi.org/10.1073/pnas.0906044106

Etheridge, D. M., Steele, L. P., Langenfelds, R. L., Francey, R. J., Barnola, J. M., & Morgan, V. (1998). Historical CO_2 records from the Law Dome DE08, DE08-2, and DSS ice cores. *Trends: a compendium of data on global change*, 351–364.

Fabry, V. J., Seibel, B. A., Feely, R. A., & Orr, J. C. (2008). Impacts of ocean acidification on marine fauna and ecosystem processes. *ICES Journal of Marine Science*, *65*(3), 414–432. https://doi.org/10.1093/icesjms/fsn048

Foster, G. L., & Rae, J. W. (2016). Reconstructing ocean pH with boron isotopes in foraminifera. *Annual Review of Earth and Planetary Sciences*, *44*, 207–237. https://doi.org/10.1146/annurev-earth-060115-012226

Gattuso, J.-P., Magnan, A., Billé, R., Cheung, W. W. L., Howes, E. L., Joos, F., et al. (2015). Contrasting futures for ocean and society from different anthropogenic CO_2 emissions scenarios. *Science*, *349*(6243), 4722–7726. https://doi.org/10.1126/science.aac4722

Gordon, L. I., & Jones, L. B. (1973). The effect of temperature on carbon dioxide partial pressures in seawater. *Marine Chemistry*, *1*(4), 317–322. https://doi.org/10.1016/0304-4203(73)90021-2

Grove, J. M. (1988). *The Little Ice Age*. New York: Methuen.

Gruber, N., Clement, D., Carter, B. R., Feely, R. A., van Heuven, S., Hoppema, M., et al. (2019). The ocean sink for anthropogenic CO_2 from 1994 to 2007. *Science*, *363*(6432), 1193–1199. https://doi.org/10.1126/science.aau5153

Guinotte, J. M., & Fabry, V. J. (2008). Ocean acidification and its potential effects on marine ecosystems. *Annals of the New York Academy of Sciences*, *1134*, 320–342. https://doi.org/10.1196/annals.1439.013

Haase-Schramm, A., Böhm, F., Eisenhauer, A., Dullo, W. C., Joachimski, M. M., Hansen, B., & Reitner, J. (2003). Sr/Ca ratios and oxygen isotopes from sclerosponges: Temperature history of the Caribbean mixed layer and thermocline during the Little Ice Age. *Paleoceanography and Paleoclimatology*, *18*(3), 1073. https://doi.org/10.1029/2002PA000830

Haug, G. H., Gunther, D., Peterson, L. C., Sigman, D. M., Hughen, K. A., & Aeschlimann, B. (2003). Climate and the collapse of Maya Civilization. *Science*, *299*(5613), 1731–1735. https://doi.org/10.1126/science.1080444

Haug, G. H., Hughen, K. A., Sigman, D. M., Peterson, L. C., & Rohl, U. (2001). Southward migration of the Intertropical Convergence Zone through the Holocene. *Science*, *293*, 1304–1308.

Hemming, N. G., & Hanson, G. N. (1992). Boron isotopic composition and concentration in modern marine carbonates. *Geochimica et Cosmochimica Acta*, *56*(1), 537–543. https://doi.org/10.1016/0016-7037(92)90151-8

Henehan, M. J., Evans, D., Shankle, M., Burke, J. E., Foster, G. L., Anagnostou, E., et al. (2017). Size-dependent response of foraminiferal calcification to seawater carbonate chemistry. *Biogeosciences*, *14*, 3287–3308. https://doi.org/10.5194/bg-14-3287-2017

Henehan, M. J., Foster, G. L., Rae, J. W., Prentice, K. C., Erez, J., Bostock, H. C., et al. (2015). Evaluating the utility of B/Ca ratios in planktic foraminifera as a proxy for the carbonate system: A case study of *Globigerinoides ruber*. *Geochemistry, Geophysics, Geosystems*, *16*, 1052–1069. https://doi.org/10.1002/2014GC005514

Hodell, D. A., Brenner, M., Curtis, J. H., Medina-Gonzalez, R., Eldefonso-Chan Can, E., Albornaz-Pat, A., & Guilderson, T. P. (2005). Climate change on the Yucatan Peninsula during the Little Ice Age. *Quaternary Research*, *63*, 109–121.

Holm, S. (1979). A simple sequentially rejective multiple test procedure. *Scandinavian journal of statistics*, 65–70.

Hönisch, B., & Hemming, N. G. (2004). Ground-truthing the boron isotope-paleo-pH proxy in planktonic foraminifera shells: Partial dissolution and shell size effects. *Paleoceanography*, *19*, PA4010. https://doi.org/10.1029/2004PA001026

Hughen, K. A., Overpeck, J. T., Lehman, S. J., Kashgarian, M., Southon, J., Peterson, L. C., et al. (1998). Deglacial changes in ocean circulation from an extended radiocarbon calibration. *Nature*, *391*(6662), 65. https://doi.org/10.1038/34150

Hughen, K. A., Overpeck, J. T., Peterson, L. C., & Anderson, R. F. (1996). The nature of varved sedimentation in the Cariaco Basin, Venezuela, and its palaeoclimatic significance. *Geological Society, London, Special Publications*, *116*(1), 171–183. https://doi.org/10.1144/GSL.SP.1996.116.01.15

Keeling, C. D. (1979). The Suess effect: ^{13}Carbon-^{14}Carbon interrelations. *Environment International*, *2*(4-6), 229–300. https://doi.org/10.1016/0160-4120(79)90005-9

Keigwin, L. D. (1996). The Little Ice Age and Medieval Warm Period in the Sargasso Sea. *Science*, *274*(5292), 1504–1508. https://doi.org/10.1126/science.274.5292.1504

Khatiwala, S., Tanhua, T., Mikaloff Fletcher, S., Gerber, M., Doney, S. C., Graven, H. D., et al. (2013). Global ocean storage of anthropogenic carbon. *Biogeosciences*, *10*(4), 2169–2191. https://doi.org/10.5194/bg-10-2169-2013

Kroeker, K. J., Kordas, R. L., Crim, R. N., & Singh, G. G. (2010). Meta-analysis reveals negative yet variable effects of ocean acidification on marine organisms. *Ecology Letters*, *13*(11), 1419–1434. https://doi.org/10.1111/j.1461-0248.2010.01518.x

Lane, C. S., Horn, S. P., Orvis, K. H., & Thomason, J. M. (2011). Oxygen isotope evidence of Little Ice Age aridity on the Caribbean slope of the Cordilla Central, Dominican Republic. *Quaternary Research*, *75*, 461–470. https://doi.org/10.1016/j.yqres.2011.01.002

Lewis, E., Wallace, D. & Allison, L.J. (1998). Program developed for CO2 system calculations. Carbon Dioxide Information Analysis Center, managed by Lockheed Martin Energy Research Corporation for the US Department of Energy Tennessee.

Lohmann, G. P. (1995). A model for variation in the chemistry of planktonic foraminifera due to secondary calcification and selective dissolution. *Paleoceanography*, *10*, 445–457. https://doi.org/10.1029/95PA00059

Lombard, F., Erez, J., Michel, E., & Labeyrie, L. (2009). Temperature effect on respiration and photosynthesis of the symbionts-bearing planktonic foraminifera *Globigerinoides ruber*, *Orbulina universa*, and *Globigerinella siphonifera*. *Limnology and Oceanography*, *54*(1), 210–218. https://doi.org/10.4319/lo.2009.54.1.0210

Lorenzoni, L. (2005). *The influence of local rivers on the eastern Cariaco Basin, Venezuela (unpublished masters dissertation)*. Tampa, FL. Retrieved from: University of South Florida. https://scholarcommons.usf.edu/etd/747/

Lorenzoni, L., Thunell, R. C., Benitez-Nelson, C. R., Hollander, D., Martinez, N., Tappa, E., et al. (2009). The importance of subsurface nepheloid layers in transport and delivery of sediments to the eastern Cariaco Basin, Venezuela. *Deep Sea Research Part I: Oceanographic Research Papers*, *56*(12), 2249–2262. https://doi.org/10.1016/j.dsr.2009.08.001

Mann, M. E., Zhang, Z., Rutherford, S., Bradley, R. S., Hughes, M. K., Shundell, D., et al. (2009). Global signatures and dynamical origins of the Little Icea Age and Medieval Climate Anomaly. *Science*, *326*(5957), 1256–1260. https://doi.org/10.1126/science.1177303

Marshall, B. J., Thunell, R. C., Henehan, M. J., Astor, Y., & Wejnert, K. E. (2013). Planktonic foraminiferal area density as a proxy for carbonate ion concentration: A calibration study using the Cariaco Basin ocean time series. *Paleoceanography*, *28*, 363–376. https://doi.org/10.1002/palo.20034

Marshall, B. J., Thunell, R. C., Spero, H. J., Henehan, M. J., Lorenzoni, L., & Astor, Y. (2015). Morphometric and stable isotopic differentiation of Orbulina universa morphotypes from the Cariaco Basin, Venezuela. *Marine Micropaleontology*, *120*, 46–64. https://doi.org/10.1016/j.marmicro.2015.08.001

Mehrbach, C., Culberson, C. H., Hawley, J. E., & Pytkowicx, R. M. (1973). Measurement of the apparent dissociation constants of carbonic acid in seawater at atmospheric pressure 1. *Limnology and Oceanography*, *18*(6), 897–907. https://doi.org/10.4319/lo.1973.18.6.0897

Moberg, F., & Folke, C. (1999). Ecological goods and services of coral reef ecosystems. *Ecological Economics*, *29*(2), 215–233. https://doi.org/10.1016/S0921-8009(99)00009-9

Morrison, J. M., & Smith, O. P. (1990). Geostrophic transport variability along the Aves Ridge in the eastern Caribbean Sea during 1985–1986. *Journal of Geophysical Research*, *95*(C1), 699–710. https://doi.org/10.1029/JC095iC01p00699

Moy, A. D., Howard, W. R., Bray, S. G., & Trull, T. W. (2009). Reduced calcification in Modern Southern Ocean planktonic foraminifera. *Nature Geoscience*, *2*(4), 276. https://doi.org/10.1038/ngeo460

Muller-Karger, F., Varela, R., Thunell, R., Astor, Y., Zhang, H., Luerssen, R., & Hu, C. (2004). Processes of coastal upwelling and carbon flux in the Cariaco Basin. *Deep Sea Research Part II: Topical Studies in Oceanography*, *51*(10-11), 927–943. https://doi.org/10.1016/j.dsr2.2003.10.010

Muller-Karger, F. E., Astor, Y. M., Benitez-Nelson, C. R., Buck, K. N., Fanning, K. A., Lorenzoni, L., et al. (2019). The scientific legacy of the CARIACO Ocean time-series program. *Annual Review of Marine Science*, *11*, 413–437. https://doi.org/10.1146/annurev-marine-010318-095150

Muller-Karger, F. E., & Castro, R. A. (1994). Mesoscale processes affecting phytoplankton abundance in the southern Caribbean Sea. *Continental Shelf Research*, *14*(2-3), 199–221. https://doi.org/10.1016/0278-4343(94)90013-2

Naik, S. S., Godad, S. P., & Naidu, P. D. (2011). Does carbonate ion control planktonic foraminifera shell calcification in upwelling regions? *Current Science*, *101*(10), 1370–1375.

Naik, S. S., Godad, S. P., Naidu, P. D., & Ramaswamy, V. (2013). A comparison of *Globigerinoides ruber* calcification between upwelling and non-upwelling regions in the Arabian Sea. *Journal of Earth System Science*, *122*(4), 1153–1159. https://doi.org/10.1007/s12040-013-0330-y

NOAA. (2016). Annual mean carbon dioxide concentrations for Mauna Loa, Hawaii https://www.esrl.noaa.gov/gmd/ccgg/trends/monthly.html. Accessed 5/18/19.

Orr, J. C., Fabry, V. J., Aumont, O., Bopp, L., Doney, S. C., Feely, R. A., et al. (2005). Anthropogenic ocean acidification over the twenty-first century and its impact on calcifying organisms. *Nature*, *437*(7059), 681–686. https://doi.org/10.1038/nature04095

Osborne, E. B., Thunell, R. C., Marshall, B. J., Holm, J. A., Tappa, E. J., Benitez-Nelson, C., et al. (2016). Calcification of the planktonic foraminifera Globigerina bulloides and carbonate ion concentration: Results from the Santa Barbara Basin. *Paleoceanography*, *31*, 1083–1102. https://doi.org/10.1002/2016PA002933

Peterson, L. C., & Haug, G. H. (2006). Variability in the mean latitude of the Atlantic Intertropical Convergence Zone as recorded by riverine input of sediments to the Cariaco Basin (Venezuela). *Palaeogeography, Palaeoclimatology, Palaeoecology*, *234*(1), 97–113. https://doi.org/10.1016/j.palaeo.2005.10.021

Peterson, L. C., Overpeck, J. T., Kipp, N. G., & Imbrie, J. (1991). A high-resolution late Quaternary upwelling record from the anoxic Cariaco Basin, Venezuela. *Paleoceanography and Paleoclimatology*, *6*(1), 99–119. https://doi.org/10.1029/90PA02497

R Core Team (2018). *R: A language and environment for statistical computing*. Vienna, Austria: R Foundation for Statistical Computing.

Rebotim, A., Voelker, A. H. L., Jonkers, L., Waniek, J. J., Meggers, H., Schiebel, R., et al. (2017). Factors controlling the depth habitat of planktonic foraminifera in the subtropical eastern North Atlantic. *Biogeosciences*, *14*(4), 827–859. https://doi.org/10.5194/bg-14827-2017

Revelle, W. (2018). psych: Procedures for personality and psychological research, Northwestern University, Evanston, IL, USA. http://CRAN.R-project.org/package=psych.

Richey, J. N., Thirumalai, K., Khider, D., Reynolds, C. E., Partin, J. W., & Quinn, T. M. (2019). Consideration for *Globigerinoides ruber* (white and pink) paleoceanography: Comprehensive insights from a long-running sediment trap. *Paleoceanography and Paleoclimatology*, *34*, 1–21. https://doi.org/10.1029/2018PA003417

Ridgewell, A., & Zeebe, R. E. (2005). The role of the global carbonate cycle in the regulation and evolution of the Earth system. *Earth and Planetary Science Letters*, *234*(3-4), 299–315. https://doi.org/10.1016/j.epsl.2005.03.006

Ries, J. B., Cohen, A. L., & McCorkle, D. C. (2009). Marine calcifiers exhibit mixed responses to CO2-induced ocean acidification. *Geology*, *37*(12), 1131–1134. https://doi.org/10.1130/G30210A.1

Roberts, J. M., Wheeler, A. J., & Freiwald, A. (2006). Reefs of the deep: the biology and geology of cold-water coral ecosystems. *Science*, *312*(5773), 543–547. https://doi.org/10.1126/science.1119861

Russell, A. D., Hönisch, B., Spero, H. J., & Lea, D. W. (2004). Effects of seawater carbonate ion concentration and temperature on shell U, Mg, and Sr in cultured planktonic foraminifera. *Geochimica et Cosmochimica Acta*, *68*(21), 4347–4361. https://doi.org/10.1016/j.gca.2004.03.013

Sabine, C. L., Feely, R. A., Gruber, N., Key, R. M., Lee, K., Bullister, J. L., et al. (2004). The oceanic sink for anthropogenic CO_2. *Science*, *305*(5682), 367–371. https://doi.org/10.1126/science.1097403

Sanyal, A., Bijma, J., Spero, H., & Lea, D. W. (2001). Empirical relationship between pH and the boron isotopic composition of Globigerinoides sacculifer: Implications for the boron isotope paleo-pH proxy. *Paleoceanography*, *16*(5), 515–519. https://doi.org/10.1029/2000PA000547

Sanyal, A., Hemming, N. G., Broecker, W. S., Lea, D. W., Spero, H. J., & Hanson, G. N. (1996). Oceanic pH control on the boron isotopic composition of foraminifera: evidence from culture experiments. *Paleoceanography*, *11*(5), 513–517. https://doi.org/10.1029/96PA01858

Schiebel, R. (2002). Planktic foraminiferal sedimentation and the marine calcite budget. *Global Biogeochemical Cycles*, *16*(4), 1065. https://doi.org/10.1029/2001GB001459

Schmidt, D. N., Renaud, S., Bollmann, J., Schiebel, R., & Thierstein, H. R. (2004). Size distribution of Holocene planktic foraminifer assemblages: Biogeography, ecology and adaptation. *Marine Micropaleontology*, *50*(3), 319–338. https://doi.org/10.1016/S0377-8398(03)00098-7

Takahashi, T., Olafsson, J., Goddard, J. G., Chipman, D. W., & Sutherland, S. C. (1993). Seasonal variation of CO_2 and nutrients in the high-latitude surface oceans: A comparative study. *Global Biogeochemical Cycles*, *7*(4), 843–878. https://doi.org/10.1029/93GB02263

Takahashi, T., Williams, R. T., & Bos, D. L. (1982). Carbonate chemistry GEOSECS Pacific Expedition, 3. Hydrographic Data WS Broecker, DW Spencer, H. Craig, 78-82.

Taylor, G. T., Muller-Karger, F. E., Thunell, R. C., Scranton, M. I., Astor, Y., Varela, R., et al. (2019). Ecosystem responses in the southern Caribbean Sea to global climate change. *Proceedings of the National Academy of Sciences*, *109*(47), 19,315–19,320.

Tedesco, K., & Thunell, R. (2003). High resolution tropical climate record for the last 6,000 years. *Geophysical Research Letters*, *30*(17), 1891. https://doi.org/10.1029/2003GL017959

Tedesco, K., Thunell, R., Astor, Y., & Muller-Karger, F. (2007). The oxygen isotope composition of planktonic foraminifera from the Cariaco Basin, Venezuela: Seasonal and interannual variations. *Marine Micropaleontology*, *62*(3), 180–193. https://doi.org/10.1016/j.marmicro.2006.08.002

Weinkauf, M. F. G., Kunze, J. G., Waniek, J. J., & Kucera, M. (2016). Seasonal variation in shell calcification of planktonic foraminifera in the NE Atlantic reveals species-specific response to temperature, productivity, and optimum growth conditions. *PLoS ONE*, *11*(2), e0148363.

Wejnert, K. E., Thunell, R. C., & Astor, Y. (2013). Comparison of species-specific oxygen isotope paleotemperature equations: Sensitivity analysis using planktonic foraminifera from the Cariaco Basin, Venezuela. *Marine Micropaleontology*, *101*, 76–88. https://doi.org/10.1016/j.marmicro.2013.03.001

Wurtzel, J. B., Black, D. E., Thunell, R. C., Peterson, L. C., Tappa, E. J., & Rahman, S. (2013). Mechanisms of southern Caribbean SST variability over the last two millennia. *Geophysical Research Letters*, *40*, 5954–5958. https://doi.org/10.1002/2013GL058458

Yu, J., Elderfield, H., & Hönisch, B. (2007). B/Ca in planktonic foraminifera as a proxy for surface seawater pH. *Paleoceanography*, *22*, PA2202. https://doi.org/10.1029/2006PA001347